# Diffraction of light by the cuticle structure of hair

HERSCHEL C. BURSTYN and YASH K. KAMATH,

*TRI/Princeton, 601 Prospect Ave., Princeton, NJ 08542.*

### Synopsis

Under a microscope, hair looks like a surface relief grating with an irregular sawtooth profile. Using scalar diffraction theory, we model what has been, until now, assumed to be a specular peak in the light scattering data. Diffraction efficiencies are calculated as a function of cuticle thickness. Convolution with apertures and Gaussian processes yields a picture that is consistent with the observed position and structure of the "specular" peak. When the cuticle thickness fails to satisfy the blaze condition, the scattered light is distributed amongst multiple diffraction orders giving rise to a complex central structure.

## INTRODUCTION

Reflection of light occurs at points where there are discontinuities in the index of refraction. Typically these occur at interfaces with air. In hair this region occurs at the surface of the cuticle (small shingles that cover the hair shaft). This observation has been used to quantify hair luster. The models that have been used to interpret the data have been based upon geometrical optics. The rake angle of the cuticle relative to the longitudinal axis of the hair, $\gamma$, is measured by determining the "scattering angle" twice: first with the hair oriented from root to tip, and then from tip to root. The difference in these two directions is equal to four times the rake angle (as the deviation from the "expected direction" in each case is twice the rake angle). The geometrical optic interpretation of the rake angle is demonstrated in Figure 1.

If one models the hair as a grating, the angles into which diffraction occurs are fixed by the periodicity. This model is motivated by micrographs of which Figure 2 is one example. However, the energy that appears in any given order will depend upon the grating depth. It is this shift in the energy distribution that yields a perceived shift in the angle of "specular" reflection. It also explains why the specular assumption yields a rake angle estimator that can be a few tenths of a degree in error. This can be shown using scalar diffraction theory. The redistribution of energy amongst the diffraction orders, also expresses itself as changes in the shape of the peak, something that has been ignored to date.

## THEORY

We start with the development of the grating equation (1). Only at specific angles does the light reflected off the facet surfaces add coherently. This can be seen in the Figure 3.
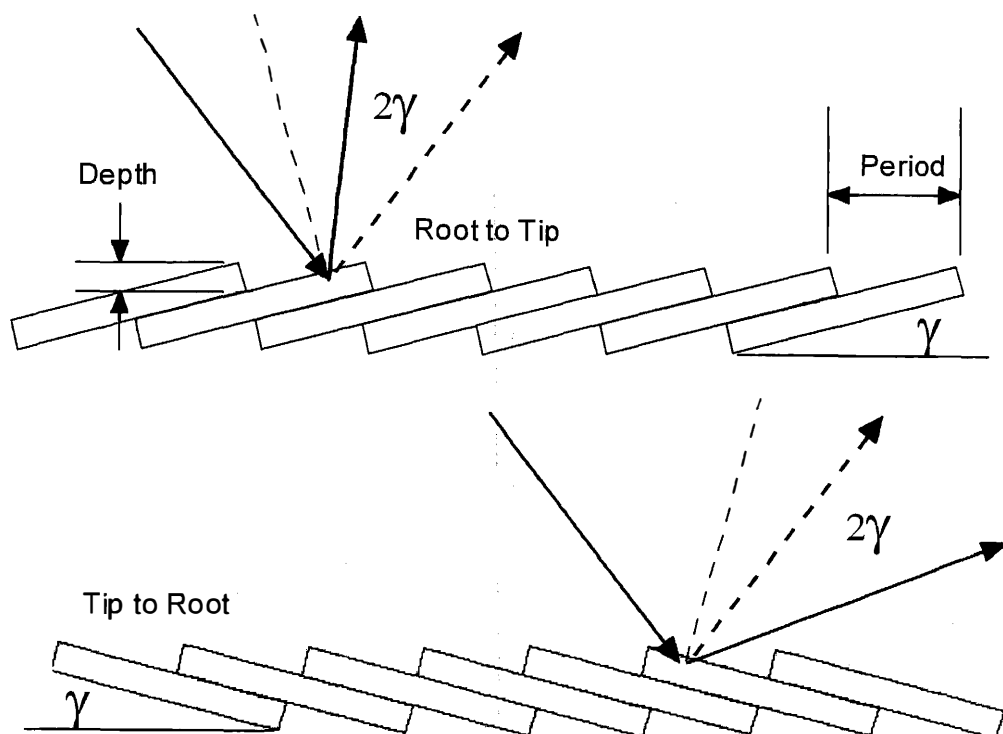
**Figure 1.** A depiction of the surface of a hair, showing: the rake angle $\gamma$. The normal the cuticle is shown as a dashed line. The "expected reflection direction" is shown in blue. The outgoing direction of the outgoing beam is deviated by $2\gamma$ in each case, as shown above. The effective period is the revealed face of the cuticle, and the depth of the grating is simply the thickness of a cuticle.

The condition is that:
$$P \sin \Theta = m\lambda. \tag{1a}$$

More generally we have,
$$\Delta\beta = \sin\Theta_{incident} - \sin\Theta_{diffracted} = \frac{m\lambda}{P} = \frac{mK}{k}. \tag{1b}$$

The integer, m, specifies the diffraction order (0, $\pm1$, $\pm2$, $\pm3$, etc.). The wavelength of the light is $\lambda$, while $k = 2\pi/\lambda$ is the associated wavevector. The grating period is denoted with P, while $K = 2\pi/P$ is defined as the grating wavevector.

We can find an expression for the optical electrical field by noting how the grating affects the incoming wave. First there is a reflection coefficient, r. This multiples the overall amplitude. There is also a reversal in direction in the y direction. Conservation of energy requires that the magnitude of the wavevector be conserved, but the grating equation indicates a change in the component in the x-direction, of mK. The product, mKx, represents the change in phase, relative to the plane that is the grating, as one scans horizontally. The phase shift due to the surface relief is simply twice the change in depth of the grating profile (round-trip distance). We use D, to represent the maximum relief. The one way phase change is then

$$\alpha = 2\pi D \Big/ \lambda. \tag{2}$$

The depth is thus measured in units of wavelength, where a one wave shift represents a change in phase of $2\pi$. The maximum round-trip phase change is $2\alpha$.

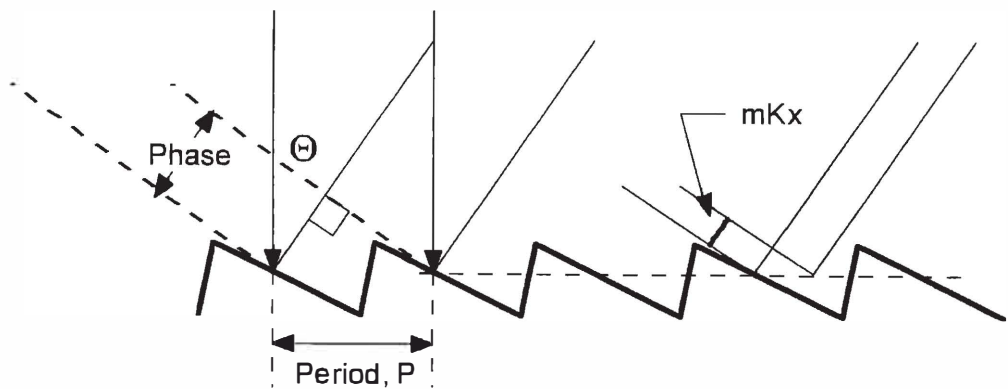**Figure 2.** A micrograph of a human hair.



**Figure 3.** Coherent reinforcement of the waves reflected from each facet occurs when the phase delay is an integral number of wavelengths.

We can now write the scalar field amplitude A, by integrating over a period (2). The contributions from all the other facets will yield the same result

$$A_m = \frac{1}{P}\int_0^P rA \exp[j(\phi(x) - nKx - \omega t)]dx = \frac{r\exp(-j\omega t)}{P}\int_0^P A\exp[j(\phi(x) - nKx)]dx.$$

where $j = (-1)^{1/2}$.

As we are using complex notation the intensity in the $m^{th}$ order is the product of the electric field with its complex conjugate, denoted as $A_m{}^*$

$$I_m = r^2 \, IA_m{}^*A_m. \tag{4}$$

We see that we do not need to explicitly carry the time and frequency information, nor do we wish to track the overall factor due to surface reflectivity. We need only consider the spatial part

$$U_m = \frac{1}{P}\int_0^P \exp[j(\phi(x) - nKx)]dx. \tag{5}$$

We evaluate $U_m$ using our phase function. The round-trip phase shift due to depth is 0 at $x = 0$, and maximum ($2\alpha$) at $x = P$. It is also linear. Substituting explicitly into equation 5 yields:
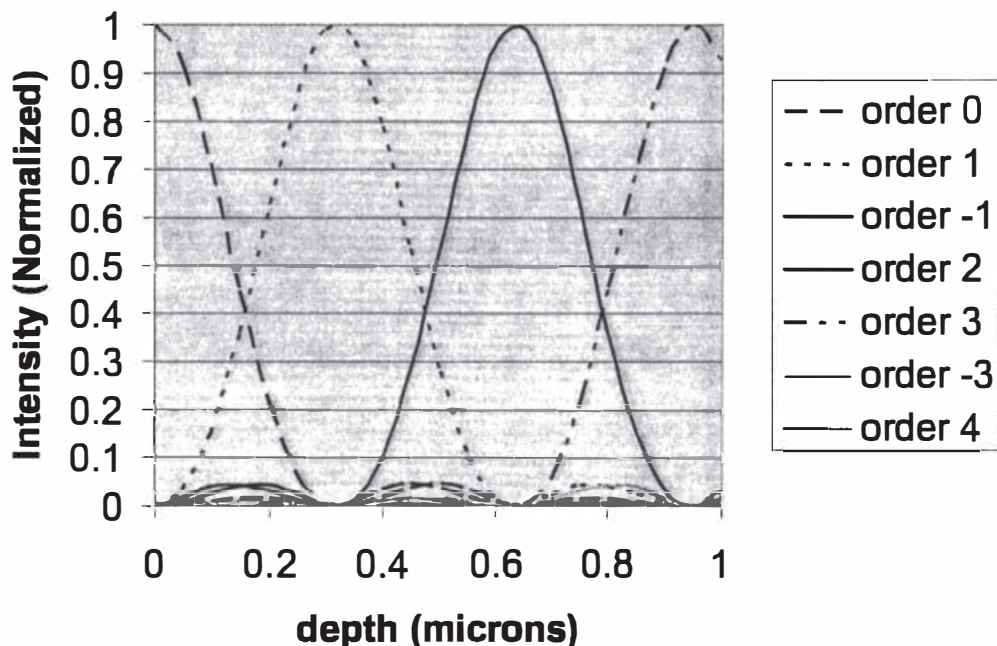
$$U_m = \frac{1}{P}\int_0^P \exp[j(2\alpha(^x/P) - nKx)]dx = \frac{1}{P}\int_0^P \exp\left[j(\alpha - m\pi)\frac{2x}{P}\right]dx \tag{6}$$

$$= \frac{j}{2(\alpha - m\pi)}\{\exp[j2(\alpha - m\pi)]-1\}.$$

Multiplying by the complex conjugate yields the intensity

$$U^*_m U_m = \frac{1}{2(\alpha - m\pi)^2}\{1 - \cos2(\alpha - m\pi)\} = \frac{1}{2(\alpha - m\pi)^2}\{1 - \cos(2\alpha)\} \tag{7}$$

$$= \frac{1}{(\alpha - m\pi)^2}\sin^2(\alpha).$$

We show a plot of this function for the significant orders in Figure 4.

The relative intensities of the various orders at a specific depth are shown in Figure 5.



Figure 4. The relative amplitude of the various orders as a function of $\alpha$. For a reasonable hair $\alpha = 10$ should correspond to a depth of about 1 micron. Notice that different orders peak at different depths and that at specific depths all the light is contained in a single order. This is the basis of blazing. Almost no light is found in negative orders.
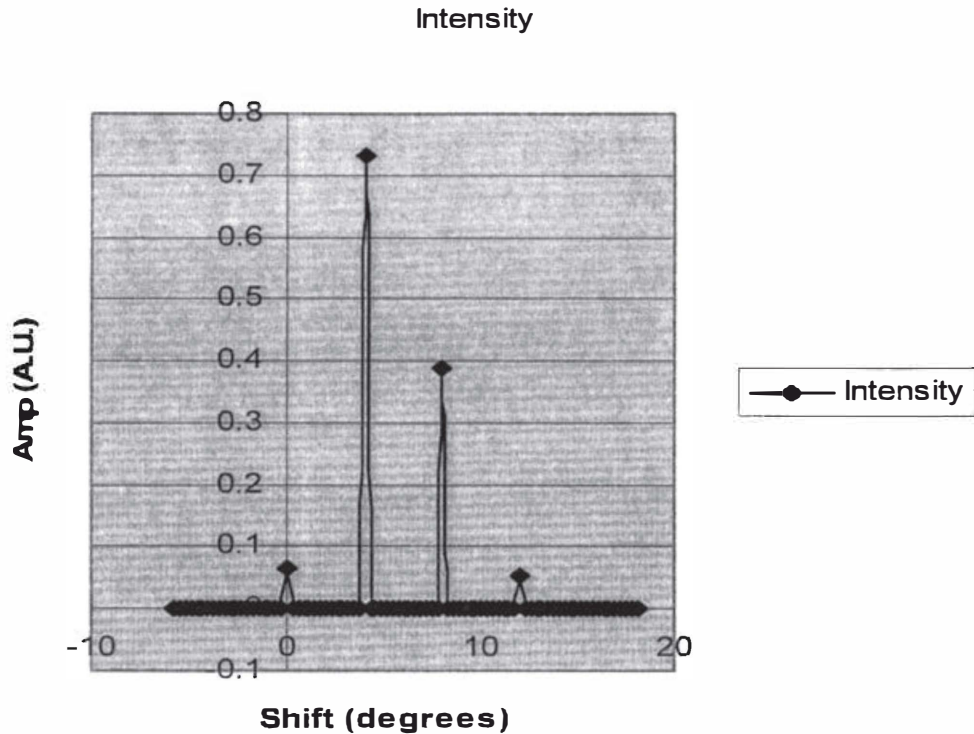
Intensity



**Figure 5.** At specific depths energy is distributed amongst a number of orders, at other depths the grating is blazed for the wavelength of interest and all the energy is contained in a single order. The position of the orders is set by the mean periodicity of the grating. Ablation will increase facet spacing variability.

## EXPERIMENTAL SIMULATION

Real experiments use lasers with Gaussian beam shapes; the illumination optics has a finite beam divergence, and the detector has finite aperture size. This means that the signal is really a convolution of the diffraction pattern with real system artifacts.

### THE DIFFRACTED ORDERS ARE SPATIALLY INCOHERENT WITH EACH OTHER

The first issue that needs to be addressed is mixing between orders. We note that the orders exit at different angles from the sample (nominally with 4 degree separations). This means that the outgoing plane waves, that are the orders, will be tilted with respect to each other. Many fringes will appear across the photosensitive surface. This means that the orders will not be spatially coherent at the detector, and any cross beating terms will explicitly cancel. We can add the intensities of the orders incoherently.

### THE LASER HAS A GAUSSIAN BEAM SHAPE

The laser beam profile is Gaussian, and as such its properties are well known. We can assume that the minimum waist is at the hair ($z = 0$) and that the electric field propagates as

$$E(r,z) = E_{\bullet} \frac{\eta_0}{\eta(z)} \exp\left[ -\frac{r^2}{\eta(z)^2} \right] \exp\left[ -j\left( kz - \arctan\left( \frac{z}{z_R} \right) + \frac{kr^2}{2R(z)} \right) \right]. \quad (8a)$$

The beam's radius $\eta$, goes as

$$\eta(z) = \eta_0 \left( 1 + \left( \frac{z}{z_R} \right)^2 \right)^{1/2},$$

where

$$z_R = \frac{\pi \eta_0^2}{\lambda}$$

is the Rayleigh range. The wavefront curvature propagates as

$$R(z) = z \left[ 1 + \left( \frac{\pi \eta_0^2}{\lambda z} \right)^2 \right]. \tag{9}$$

The Rayleigh range is that distance over which the beam does not significantly diverge. Notice that the beam is a plane wave both at focus and at infinity.

If our detector is well within the Raleigh range we can simplify the expression to

$$E(r,z) = E_0 \exp \left[ -\frac{r^2}{\eta_0^2} \right] \exp \left[ -j \left( kz - \left( \frac{z}{z_R} \right) \right) \right] \tag{8b}$$

For a beam with a waist of 1 mm = 1000 μm, the Rayleigh range of the order of 5 meters (@0.63 μm). If focused to 100 microns this reduces to 4.9 cm.

This distribution is centered upon a diffraction order which is located at $\theta_0$. As such, $r = z(\theta - \theta_0)$. We can define $\eta_0/z$ as $\Omega$ and rewrite the expression as

$$E(r,z) = E_0 \exp \left[ -\frac{(\theta - \theta_0)^2}{\Omega^2} \right] \exp \left[ -j \left( kz - \left( \frac{z}{z_R} \right) \right) \right] \tag{8c}$$

Thus we can also interpret the spatial distribution as an angular one. The propagating phase part is nominally a plane wave that will have almost no effect on the final observed intensity. The observed intensity in the plane of the detector, for a single order, will be a Gaussian distributed in angle about a direction that is specified by the grating equation.

GRATING PERIOD VARIABILITY CAN BE MODELED AS A GAUSSIAN PHASE SCREEN

We modeled the hair as a phase grating of specific period. The cuticles, as they wear, will thin and fracture. We have shown how the depth can be accounted for in a scalar diffraction theory. We need to somehow account for the increased variability in the pitch. There is however a local modulation of period. A random modulation can be accounted for by introducing a Gaussian phase screen as a transmission mask. Because the screen acts multiplicatively in real space, it appears as a convolution in the transform space (3). In other words the Gaussian profile that is the laser's beam cross-section is convoluted with phase screen's Gaussian in angle space, resulting in what may be referred to as an excess spreading about the mean (angular) position. This is explicitly expressed in the following way.

Given two Gaussian distributions,

$$p_1(x) = \frac{1}{2\pi\sigma_1} \exp\left[ -\frac{(x-\mu_1)^2}{2\sigma_1^{\,2}} \right], \qquad \text{and}$$

$$p_2(x) = \frac{2}{\pi\sigma_2} \exp\left[ -\frac{(x-\mu_2)^2}{2\sigma_2^{\,2}} \right], \tag{10}$$

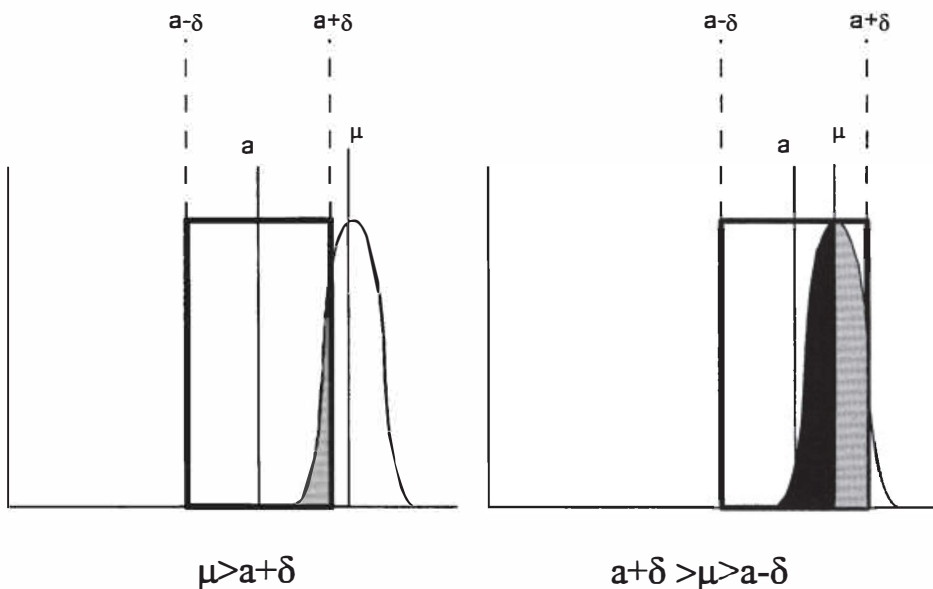their convolution is another Gaussian of broader variance

$$p_1(x)* p_2(x) = \frac{1}{2\pi(\sigma_1^{\,2}+\sigma_2^{\,2})^{1/2}} \exp\left[ -\frac{(x-\{\mu_1+\mu_2\})^2}{2(\sigma_1^{\,2}+\sigma_2^{\,2})} \right]. \tag{11}$$

In our case the mean of the process is zero. The randomness of the grating that is the hair is noticed as an excess spreading of the laser beam.

CONVOLVING THE BROADENED DIFFRACTED ORDERS WITH THE DETECTOR APERTURE

Measurement systems have finite apertures. We can assume that this aperture is a slit of angular width $2\delta$, centered about and angle, a. For any given order, the detector sees a portion of the curve under the Gaussian intensity distribution as shown in Figure 6. This leads to a sum of error functions (ERF).

$$I = \int_{a-\delta}^{a+\delta} \exp\left[ -\frac{(x-\mu_i)^2}{2\sigma^2} \right] dx = \int_{a-\delta-\mu}^{a=\delta-\mu} \exp\left[ -\frac{(z)^2}{2\sigma^2} \right] dz = \frac{1}{\sigma\sqrt{2}} \int_{\mu-\delta-a/\sigma\sqrt{2}}^{\mu+\delta-a/\sigma\sqrt{2}} \exp[-w^2] dw$$



$$\mu > a+\delta \qquad\qquad a+\delta > \mu > a-\delta$$

**Figure 6.** The integral under the Gaussian can come in as a sum or difference of error functions depending upon the position of the aperture center relative to the location of the mean, and the aperture width.

$$I_i = \frac{1}{\sigma\sqrt{2}}\left\{ERF\left(\frac{|\mu_i - a| + \delta}{\sigma\sqrt{2}}\right) - ERF\left(\frac{|\mu_i - a| - \delta}{\sigma\sqrt{2}}\right)\right\}$$

$$\text{for } |\mu - a| > \delta \qquad (12a)$$

$$I_i = \frac{1}{\sigma\sqrt{2}}\left\{ERF\left(\frac{\delta - |\mu_i - a|}{\sigma\sqrt{2}}\right) + ERF\left(\frac{|\mu_i - a| + \delta}{\sigma\sqrt{2}}\right)\right\}$$

$$\text{for } +\delta > |\mu - a| \qquad (12b)$$
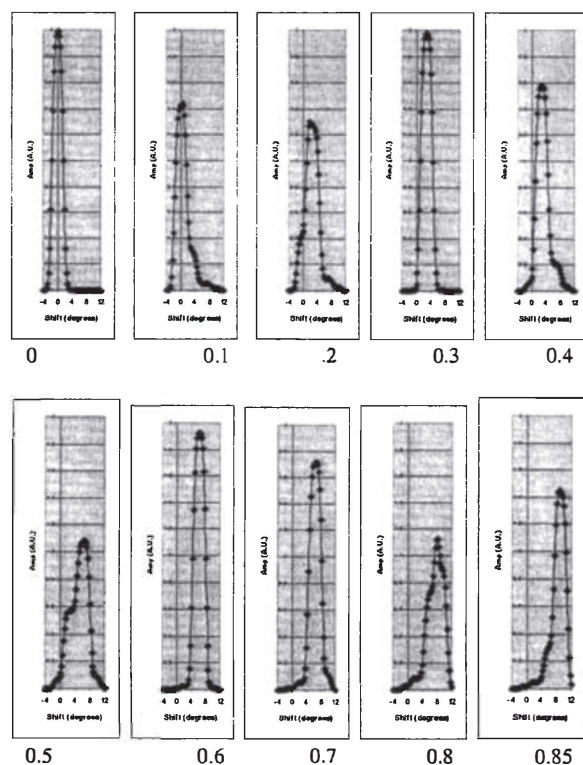
We can write this in a more compact form using the SGN function.

$$\begin{aligned}SGN(x) &= -1 \quad \text{for } x < 0 \\ &= 0 \quad \text{for } x = 0 \\ &= +1 \quad \text{for } x > 0\end{aligned} \qquad (13)$$

Let us define

$$\zeta_i = |\mu_i - a| - \delta. \qquad (14)$$

Summing over all the significant orders (to $l$), weighted by their relative intensities, we obtain



Figure 7. Intensity plotted as a function of angle for various depths. The grating period was taken to be 10 microns. The indicated depths are in microns. The areas under the curves are nearly constant.

$$I_{\text{total}} = \sum_{i=0}^{l} \frac{\sin^2\alpha}{(\alpha - i\pi)^2} \left\{ ERF\left( \zeta_i + 2\delta \middle/ \sigma\sqrt{2} \right) - SGN(\zeta_i)ERF\left( \zeta_i SGN(\zeta_i) \middle/ \sigma\sqrt{2} \right) \right\}.$$

(15)

We have implicitly integrated over a number of delta functions to obtain the above result.

We plot equation 15 for typical values. We can take the grating period to be 10 microns, spacing the orders at about 3.6 degree intervals. We can then take the aperture half-width, $\delta$, to be 0.03 radians, and the standard deviation of the Gaussian as 0.01 radians. The shape of the central peak depends upon both depth, as shown in Figure 7, and upon period, as seen in Figure 8. We can compare these plots against actual data that is traced in Figure 9, from a photogoniometer (old model).

## PRELIMINARY EXPERIMENTAL RESULTS

We have built a new photogoniometer with a 65 mW diode laser (wavelength 658 nm) from Newport Corporation having a beam diameter of 1 mm. The laser can be focused to a 100 micron lens, if required. The power has allowed us to photograph (Figure 10) the conical scattering that is characteristic of hair fibers (4). The light within the ring is considered "specular", while the light at smaller and larger radii is considered diffuse.
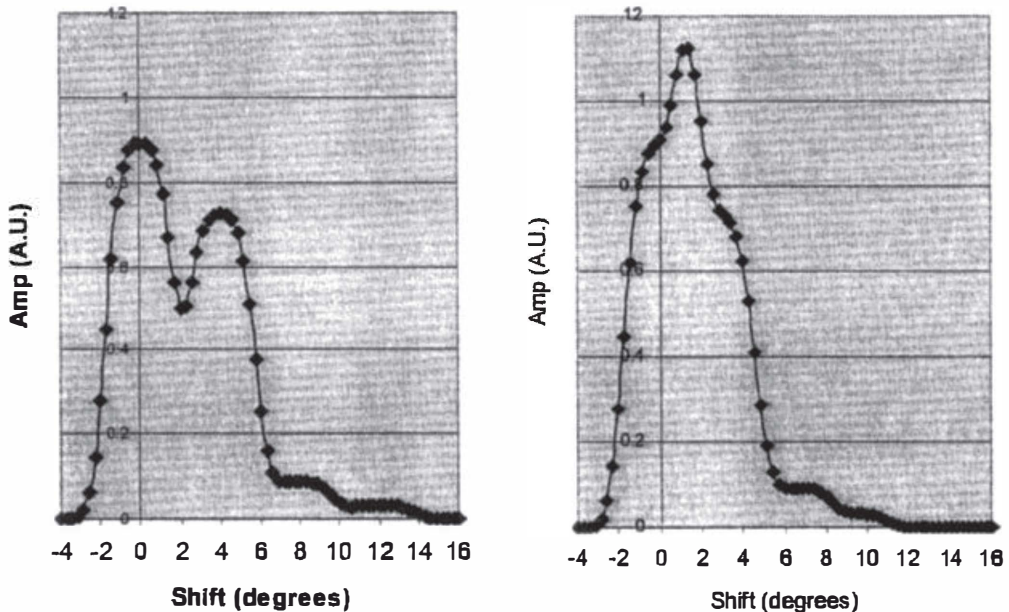


**9 microns**                **10 microns**

**Figure 8.** The grating period impacts the shape of the intensity curve. Both gratings were taken to be 0.15 microns deep. However, the curve on the left assumed a 9 micron period, while the one on the right was for a 10 micron grating. All other conditions are the same.
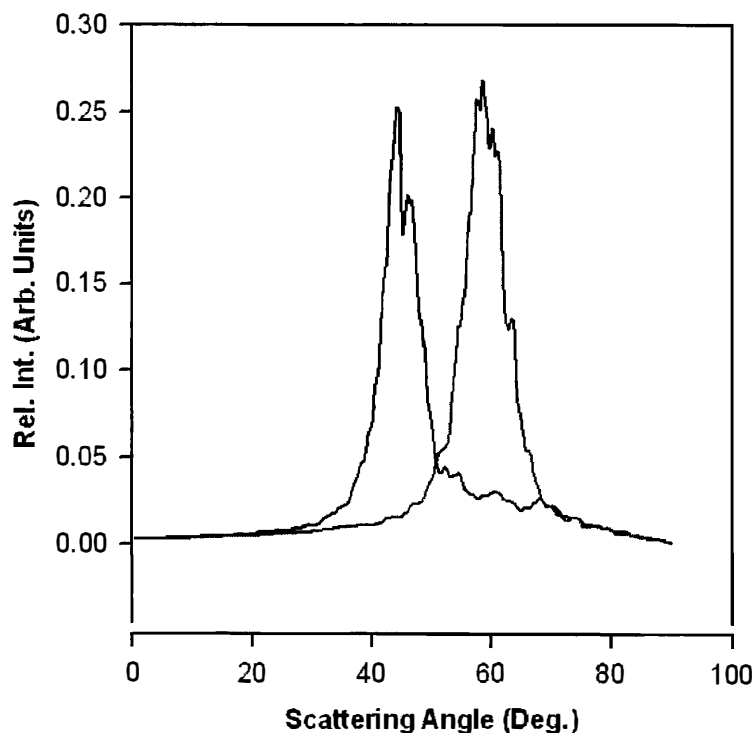
**Figure 9.** Light scattering from a human hair. One trace is taken when the hair is oriented root-to-tip, while in the other the hair is reversed. Note both the offsets in the peaks, and the structure that exists within them.

The ring has structure which can be ascribed to the grating-like structure of the assemblage of cuticles that cover the hair. Figure 11 shows this scattering in the plane of incidence.

We have observed the scattered light from a black Asian hair in the plane of incidence; first using a 2.3-mm round hole and then after stepping the aperture down to a 0.5-mm slit. The aperture was about 40-mm away from the sample. These two traces are shown in Figures 12 and 13, respectively. Figure 13 is particularly interesting because it shows that we have enough resolution to extract the diffraction data directly. We do not have to depend upon the inferences that are found in data taken with coarse apertures. The relative heights of the "diffraction" peaks tell us how thick the cuticles are. This is an indication of hair wear; assuming that the cuticles thin with abrasion or chemical attack. The width of the diffraction peaks (diffraction orders) gives us a measure of the variance in cuticle exposure. This is indicative of cuticle breakage, and thus a measure of hair damage as well. The broad background is associated with the creation of small defects, such as pitting, and has long been associated with loss of luster.

We have thus shown that various hair damage mechanisms can be observed in and extracted from the light scattering data. The problem that now needs to be addressed is the removal of instrumental artifacts.

## DECONVOLUTION

The width of the "diffraction" peaks is more than just the variance in the cuticle
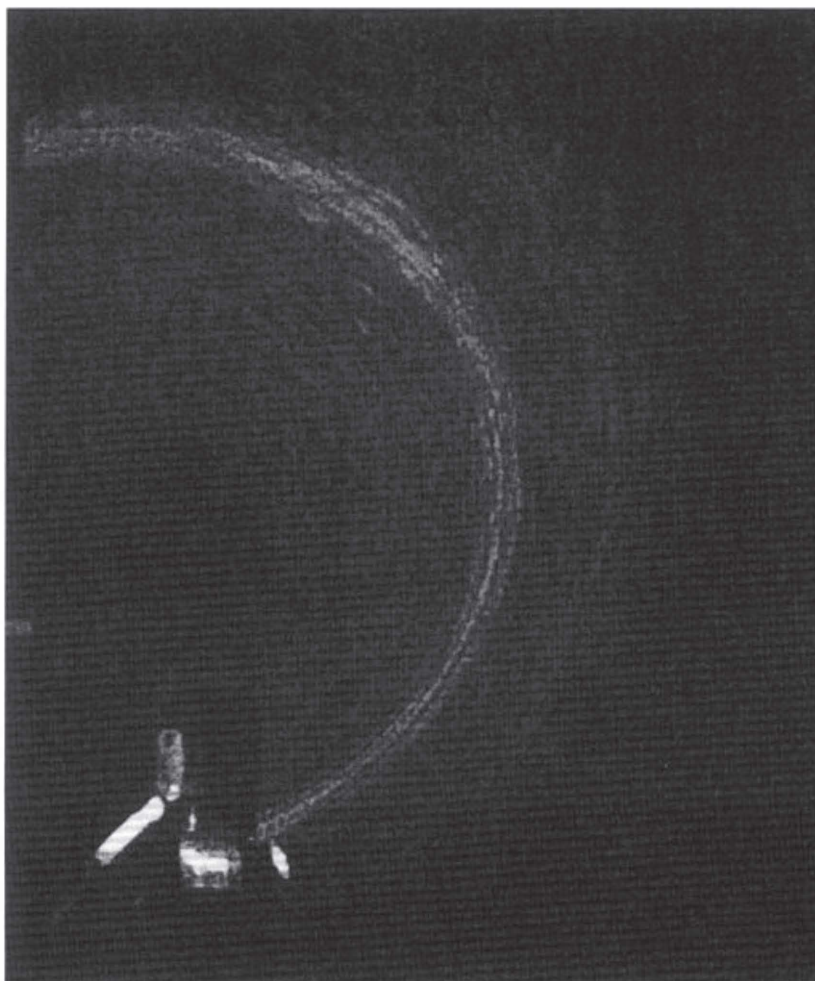
**Figure 10.** Conical light scattering from a human hair. The hair's axis is perpendicular to the plane of the circle. The hair's axis pieces the circle's center.

exposure. We have shown that the laser beam profile and aperture width are convoluted with the data. We will now show how to remove these effects.

Our exposition has indicated that the convolution should appear in the form of error functions. It may be easier to simply measure the response function of the instrument. To do this, we simply need to pass our aperture across the laser beam. We can achieve this in our system by using a wire as our sample. We can thus scan across the diffracted line or circle that arises from the wire. Such a trace, along with a picture of the light pattern is shown in Figure 14. The trace is the impulse response of the optical system, which we can call $H(\theta)$. We can take its Fourier transform, and label it $h(\omega)$. The underlying data, or signal, can be denoted as $G(\theta)$ while the raw data, $D(\theta)$ is assumed to be the convolution of the two. We thus can write

$$D(\theta) = H(\theta) \otimes G(\theta). \tag{16}$$
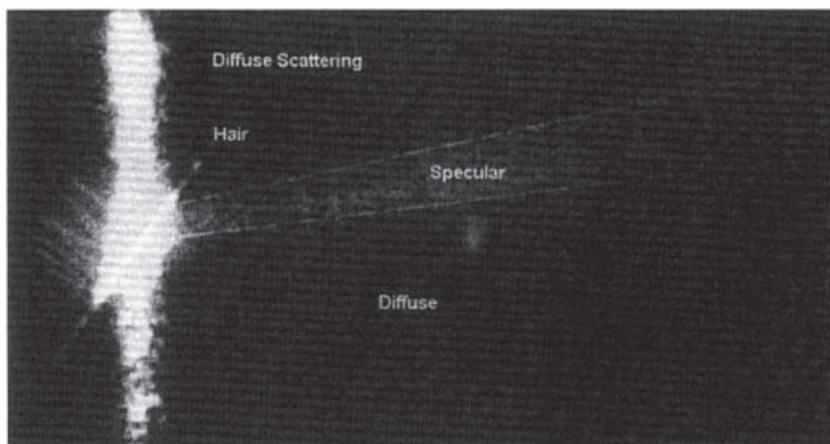
The Fourier transform then results in:

Figure 11. The light scattering as observed in the plane of incidence.
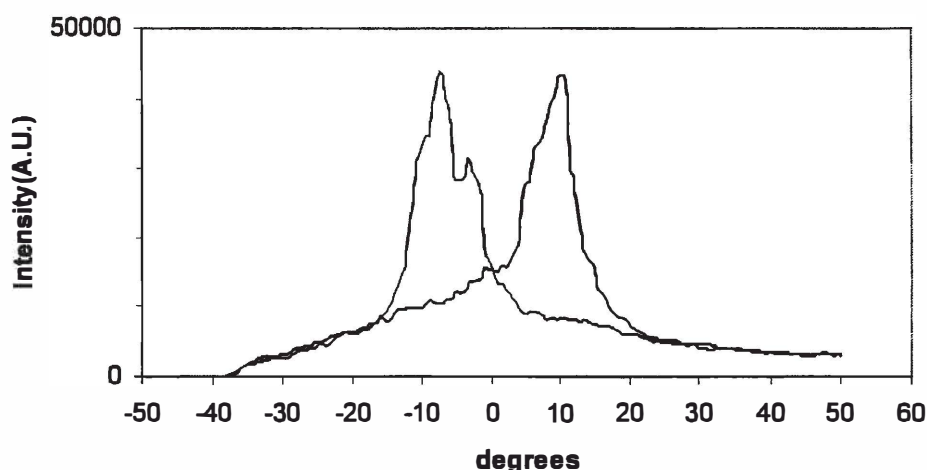


Figure 12. A trace of the scattered light from a black Asian hair, taken with the coarse aperture. Its shape is similar to what has been found historically.

$$d(\omega) = h(\omega) * g(\omega) \tag{17}$$

But as we have experimentally found the instrumental response, we can, with some restrictions, construct a frequency response $h(\omega)$ and divide it into the transform of the raw data.

$$g(\omega) = d(\omega)/h(\omega) \tag{18}$$

Transforming back into our object space yields the data, $G(\theta)$, unencumbered by instrumental broadening. We can also implement filtering algorithms in the transform space.

A word of caution needs to be made here. The variance in the cuticle spacing is fixed at any given point. This means that the signal is, in effect, fixed pattern noise. We need to sample over multiple positions on the fiber, or across different position of the ring that is the scattered light, to obtain an ensemble average.
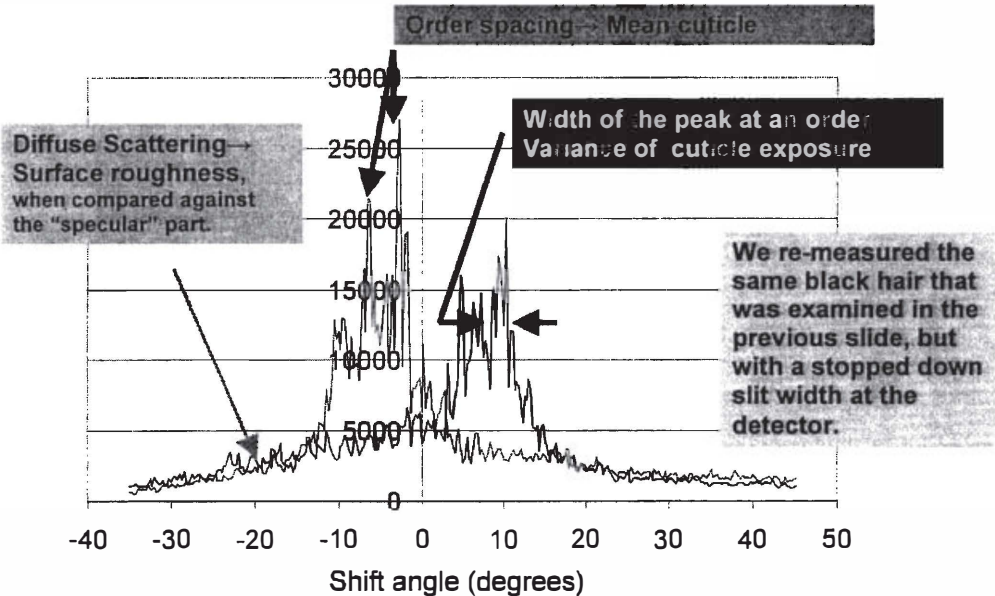
**Figure 13.** A trace of the scattered light from a black Asian hair, taken with the 500 micron slit. We can now begin to see the diffraction grating behavior that our calculations imply. The broad background is the diffuse light and due to small irregularities. The "noise" about the diffraction peaks indicates variation in cuticle exposure. The spacing between the peaks is a measure of the mean cuticle exposure. While the relative heights of the diffraction peaks allows us to extract the cuticle thickness.
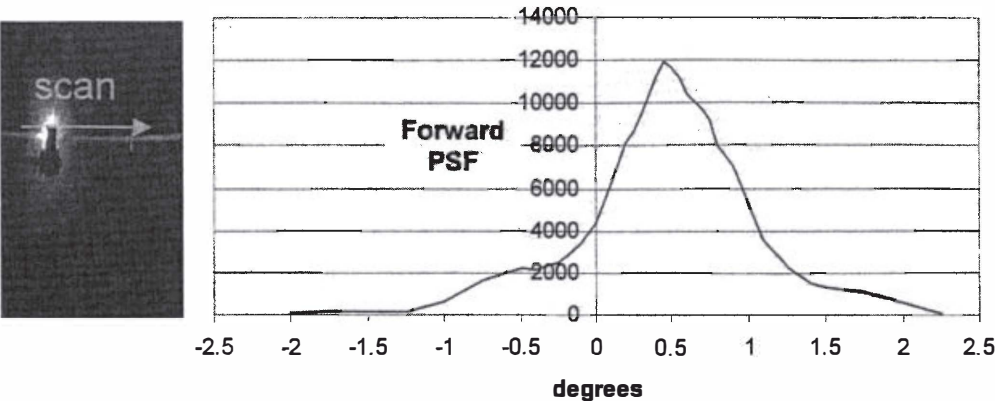


**Figure 14.** We can scan through a diffracted line to yield an estimator for the impulse response of the optical system. This can be used to deconvolute the raw data from instrumental artifacts and thus obtain a measurement of the variance of cuticle exposure and thus cuticle breakage.

## COMPARISON WITH STANDARD METHODS

It is a standard practice to derive the cuticle angle of tilt from light scattering data. The data are smoothed by fitting to a Gaussian. The centroid of the peak is often used to find the cuticle tilt angle. Geometrical optics implies that the measured shift in angle is twice this angle. It makes more sense to use a different definition for the center of the curve. Indeed a center of mass calculation suggests itself. We can find the area under the curve

and find the location that divides the area into two equal parts. This procedure works well on the simulated data, arriving at tilt angles that are within about 0.2 degrees of the input values. The error in the estimator is not statistical, but biased. It does not work for small tilt angles where almost all the energy is in the zeroth order (the intensity weighting of the orders is not linear function of depth). The errors in the estimate are comparable to those that are experimentally quoted.

## SUMMARY

The shape of the "specular" peak that one finds in light scattering experiments on hair can be explained by diffraction from the cuticle structure. The shape depends both upon the periodicity of the cuticles and their thickness. The experimental techniques that extract cuticle tilt angles assume that the positions of the scattering peaks can be determined by geometric optics. This is not supported by the analysis given here. The assumption leads to systematic errors. These experimentally quoted errors associated with these measurements are not statistical but systematic.

## REFERENCES

(1) M. V. Klein, *Optics* (John Wiley & Sons, New York, 1970), pp. 338–349.
(2) W. R. Roach, C. B. Carroll, A. R. Firester, I. Gorog, and W. Wagner, Diffraction spectrometry for videodisk quality control, *RCA Review,* **39**(3) 272 (1978).
(3) J. W. Goodman, *Introduction to Fourier Optics* (McGraw-Hill, New York, 1968).
(4) J. T. Moon and S. R. Marschner, Scattering in hair using a photon mapping approach, *Tranaction on Graphics,* **25,** 3 (Proceedings of SIGGRAPH 2006).